An Experimental Examination of Fracture Criteria Using Brittle Polystyrene

SURENDRA KUMAR GUPTA, *Mechanical Engineering Department, Rochester Institute of Technology, Rochester, New York 14623* and DAVID J. QUESNEL and JOHN LAMBROPOULOS, *Mechanical Engineering Department, University of Rochester, Rochester, NY 14627*

Synopsis

A four-point bend test was performed on injection-molded bar-shaped polystyrene specimens with notches of varying depths. The material investigated was found to be linear elastic and brittle. From the load–displacement curves, various fracture toughness parameters based on energy release rate theories and stress–intensity factors were calculated. The stress concentrations arising from the presence of finite size notches with finite root radii were also calculated. The local stress at crack initiation was found to be nearly constant for all specimens investigated while the fracture toughness parameters based on energy release rates were not constant. A distinct change in the crack propagation behavior was observed when the curvature of the stiffness vs. notch depth curve changed sign, clearly defining the onset of unstable crack growth.

INTRODUCTION

In the past three decades, fracture in metals and polymers has been studied extensively. These studies have been both experimental[1-9] and theoretical[10-15] in their approach. The outgrowth of these early works has resulted in establishment of ASTM test procedures for characterizing the fracture behavior of metals.[16,17]

One of the earliest approaches to design against fracture involved the concept of stress concentrations. The concept introduced existence of high localized stresses near a discontinuity in a structural member, such as a crack, notch, or inclusion. This high local stress σ_{max} is compared with a critical stress σ_c, and fracture is considered to occur when the critical stress is exceeded. The stress concentration factors have been computed by both analytical and numerical methods for most structural shapes and loading conditions, and are a function of geometric parameters only. An interesting treatment to this problem was by Neuber. Neuber derived analytical expressions for stress concentration factors for various load geometries as a function of the shape and size of both the specimen and the notch.[18]

Another approach, now well established, is that of stress intensity factor K, a parameter defined to represent the action of mechanical forces on any crack system. The crack tip is assumed to be sharp, and modeled as a mathematical singularity. The stress intensity fields near the crack tip under different loading modes can then be expressed as a function of the crack geometry and the applied loads.[19]

Journal of Applied Polymer Science, Vol. 32, 5585–5595 (1986)

CCC 0021-8995/86/065585-11$04.00

Fracture initiates when the stress intensity factor exceeds a critical value K_c, recognized as a material property independent of the specimen and load geometry.

Yet another approach is that of crack extension force or energy release rate G (or J), a parameter defining the strain energy released by an extending equilibrium crack.[20] Again, fracture initiates when the strain energy release rate G reaches a critical value G_c, also recognized as a material property independent of the specimen and load geometry. For an equilibrium crack in a brittle material, the two approaches K and G are equivalent,[21,22] bearing in mind that the former is the mechanistic crack tip stress intensity criterion while the latter is the macroscopic energy balance criterion. When some significant but limited plasticity is involved, the crack extension force obtains a slightly different definition and is known as J.

At present, all four concepts are used in engineering design of metallic structural members. The degree of success in predicting fracture employing any one of the above parameters is a function of the properties of the individual system. Relative to metals, little has been done in characterizing fracture behavior of polymeric materials. Kambour[23-25] and others[26-28] linked the material behavior of thermoplastic materials at the crack tip with formation of crazes, and now it is an accepted fact that new fracture surfaces form by rupture of the crazed material. The purpose of this work is to perform a comparative analysis of the four approaches for a particular brittle polymer. Based on the experience in metals, the results of this study may not be generalized.

This article will examine the fracture of brittle polystyrene using a common set of data to obtain all four parameters introduced in the foregoing paragraphs.

EXPERIMENTAL

We have chosen brittle polystyrene as the testing material for several reasons: First, polystyrene, a clear polymer, is ideal for our investigation since it can be easily machined and it allows direct observation of the fracture in the interior of the solid. Second, since it is nearly ideally brittle on the macroscopic scale, we can use linear elastic theories without considering extensive plasticity at the crack tip. Lastly, since the wave speeds and therefore the crack propagation rates are lower than in metals, particularly at small loads, we should be able to study the dynamic aspects of fracture in this material.

Polystyrene is manufactured under a variety of trade names, each with additives to modify the processing characteristics and the polymer properties. We chose Styron 678U, a general purpose polystyrene with easy flow properties.[29] The beam shaped specimens were injection molded in an ASTM die, which was endgated to produce a dominantly axial flow mode. Although residual stresses may be present at the microscopic level, they are absent on the macroscopic scale since there is no induced permanent deformation when such a specimen is, say, cut in two. Of course, these stresses can be removed by annealing, but they are regenerated upon cooling since no large range molecular motion occurs during annealing. Furthermore, the specimens are homoge-

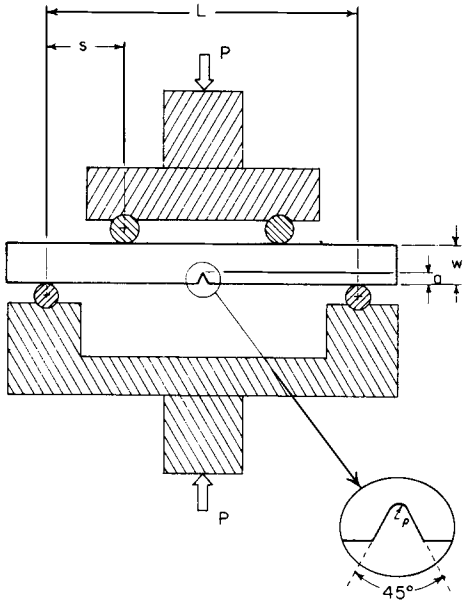

Fig. 1. Schematic of experimental four-point bending setup showing details of notch geometry. Typical specimen dimensions are 127 × 12.7 × 6.35 mm.

neous on the macroscopic scale. The bar specimens are naturally suited for bend tests. We chose four-point bend test over three-point so as to produce a well-defined stress state in a large region. In addition, previous experience has shown that this is a stable deformation geometry.[30] A V-shaped notch was introduced in each bar using a Charpy/Izod notch cutter on a horizontal bed milling machine. This provided a close control on both the notch depths (within 0.025 mm), and the notch root radius of 0.25 mm (within 0.01 mm). It was assumed that the notch was sharp enough for testing purposes. Under proper illumination at high magnifications, fracture initiation sites (crazes) were observed at the notch tip. The specimen shape, size, notch and load geometry are shown in Figure 1. For these specimens, it must be mentioned that the derivation of the stress intensity factors and the stress concentration factors is still valid as the specimens are isotropic in the plane perpendicular to the crack plane and to the crack front.

The tensile testing equipment and loading fixtures were chosen to permit loading at a constant displacement rate, and also to provide a uniform stress distribution through the specimen thickness, as well as symmetrically about the plane of the prospective crack. A MTS model 810 servo-hydraulic test frame with a 2500N full scale load cell was employed in the experiment. All tests were conducted in the lab atmosphere at room temperature in a reasonably short period of time to minimize moisture and other atmospheric effects.

Specimens with notch depths ranging from 0 to 0.7 times the specimen width (12.7 mm) were loaded on the MTS machine at a constant stroke rate of 0.00127 mm/s. Both the applied load P and the resulting displacement v of the piston were recorded in digital and analog formats. The digital recording greatly facilitated the subsequent reduction and analysis of data on a micro-

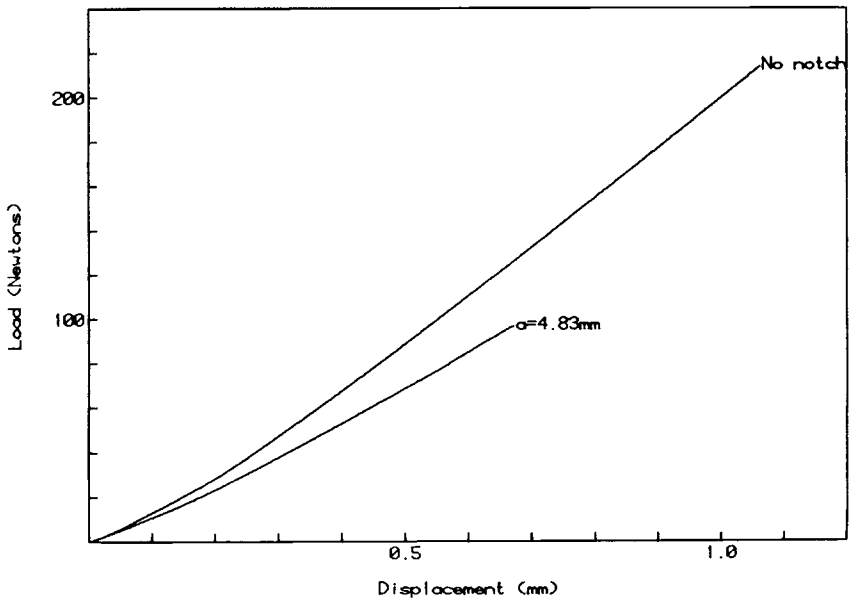

Fig. 2. Load vs. displacement plot for a notched and an unnotched specimen showing nonlinear effects at low loads due to Hertzian loading at rollers.

computer. It must be mentioned that the compliance of the testing apparatus is negligible as compared to the compliance of the specimens used.

P–v plots of a notched and an unnotched specimen are shown in Figure 2. Both the plots show an initial upward curvature while linear elasticity requires such plots to be linear. We attribute this curvature to the Hertzian loading effect at the roller pins, since upon unloading both the unnotched and notched specimens prior to fracture resulted in a linear curve which were retraced upon subsequent reloading. To subtract this effect, data correction was performed at a constant load basis. For each specimen, at regularly spaced load values, the displacement v_u of unnotched specimens was subtracted from the displacement v, and then a displacement v_1 calculated from the linear portion through the origin of the P–v plot of the unnotched specimen was added back at the same load. The resulting curves then represent the P–v variation of the specimens after the Hertzian effect has been properly removed. These curves were all linear, and the correlation coefficient in linear regression was 0.997 or better in each case. The corrected P–v curves are shown in Figure 3.

The correction procedure is well supported by comparing the compliance of the unnotched specimen as calculated from the slope of the corrected linear P–v curve (which passes through the origin) with the theoretically estimated compliance value:

$$C_{\text{exptl}} = 0.00456 \pm 0.000005 \text{ mm/N}$$

$$C_{\text{theory}} = s^2(3L - 4s)/Etw^3$$

$$= 0.00456 \text{ mm/N}$$

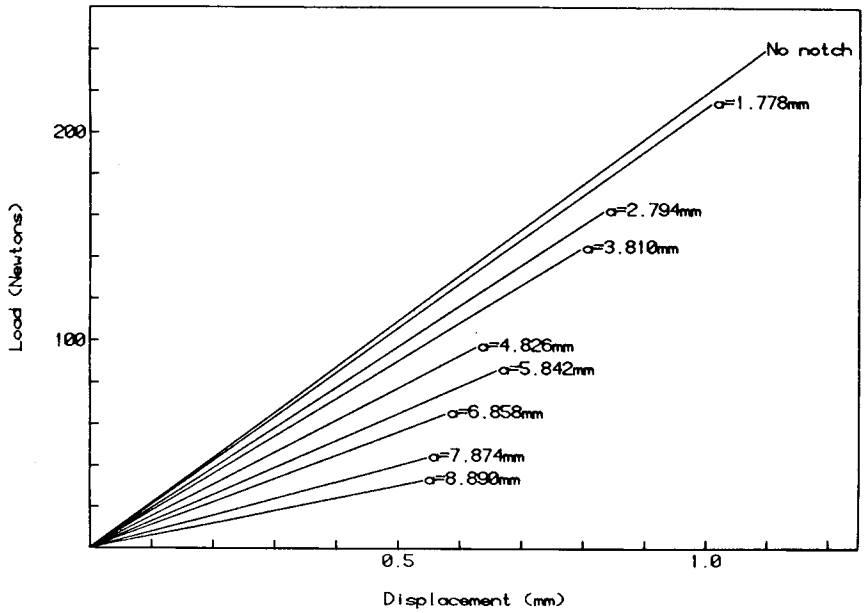

Fig. 3. Load–displacement curves for all specimens corrected for Hertzian loading effects. The corrections were made on a constant load basis. The endpoint at each curve represents the onset of fracture.

where symbols s, L, t, and w are defined in Figure 1 and E is the elastic modulus. The numerical values are

$$s = 28.75 \text{ mm}, \qquad L = 115.01 \text{ mm}, \qquad t = 6.35 \text{ mm},$$

$$w = 12.7 \text{ mm}, \qquad E = 3206 \text{ N/mm}^2 \qquad \text{(Ref. 31)}$$

For each notched specimen, a sharp load drop was recorded at fracture initiation, i.e., onset of crack growth. For specimens with notch depths smaller than 6.35 mm (specimen half-width), the crack propagated through the entire width immediately after initiation. However, for larger notch depths, the crack propagated a small distance after initiation and was arrested. A load increase was required to propagate the crack further. In no case, however, did the new load required for crack extension exceed the old load required for crack initiation. We shall comment on this phenomenon in the discussion.

RESULTS

The load P and the corrected displacement v at the onset of crack growth, henceforth referred to as P_c and v_c, respectively, are plotted as a function of notch depth a in Figures 4(a) and 4(b). Since P_c should be zero when the notch depth equals the width of the specimen, a point corresponding to this conclusion is plotted in Figure 4(a). A smooth curve has been drawn through the points using least squares smoothing by natural splines.[32] Similarly, a smooth curve has been drawn through the v_c vs. a points in the plot of Figure 4(b). While Figure 4(b) does not show an asymptote clearly, it is reasonable to

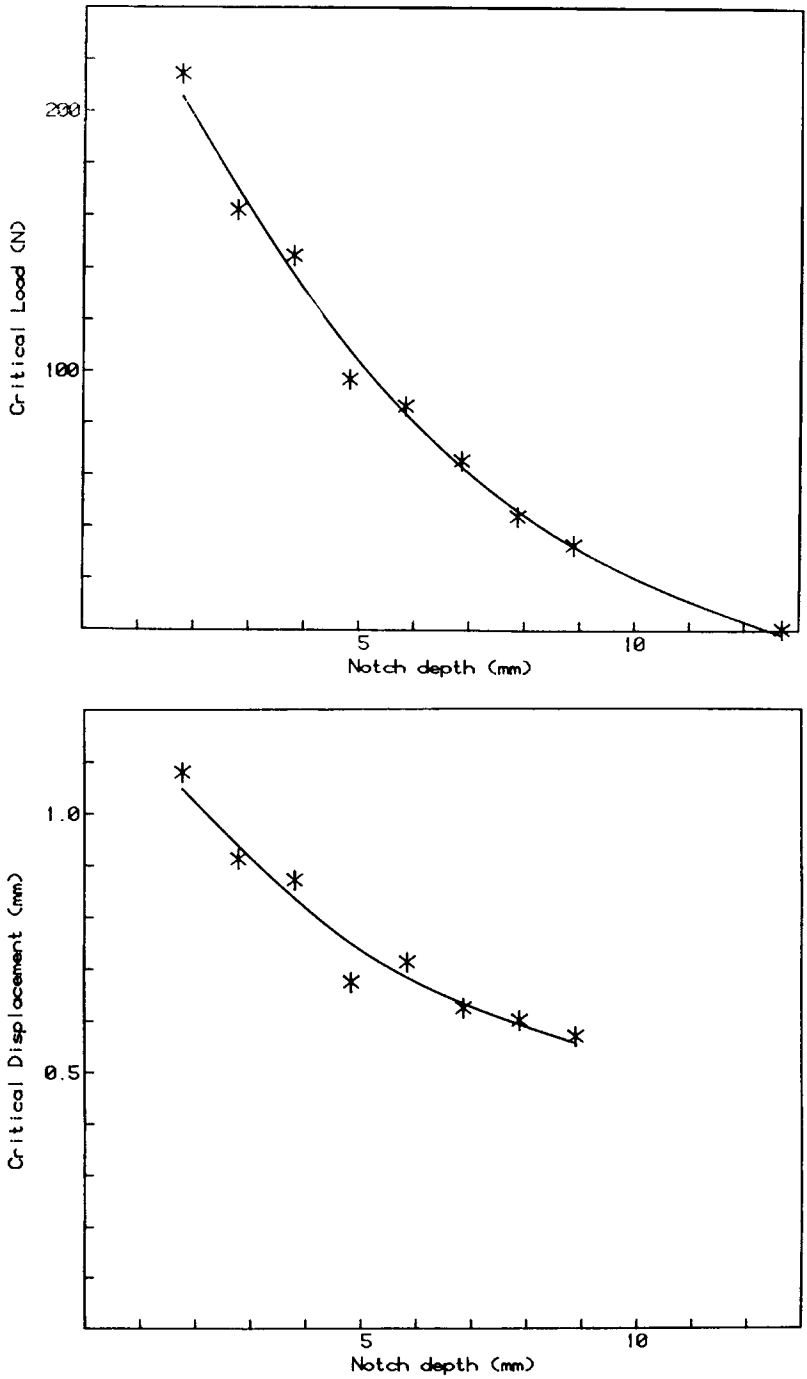

Fig. 4(a). Load as a function of notch depth at the onset of fracture. (b). Displacement as a function of notch depth at the onset of fracture.

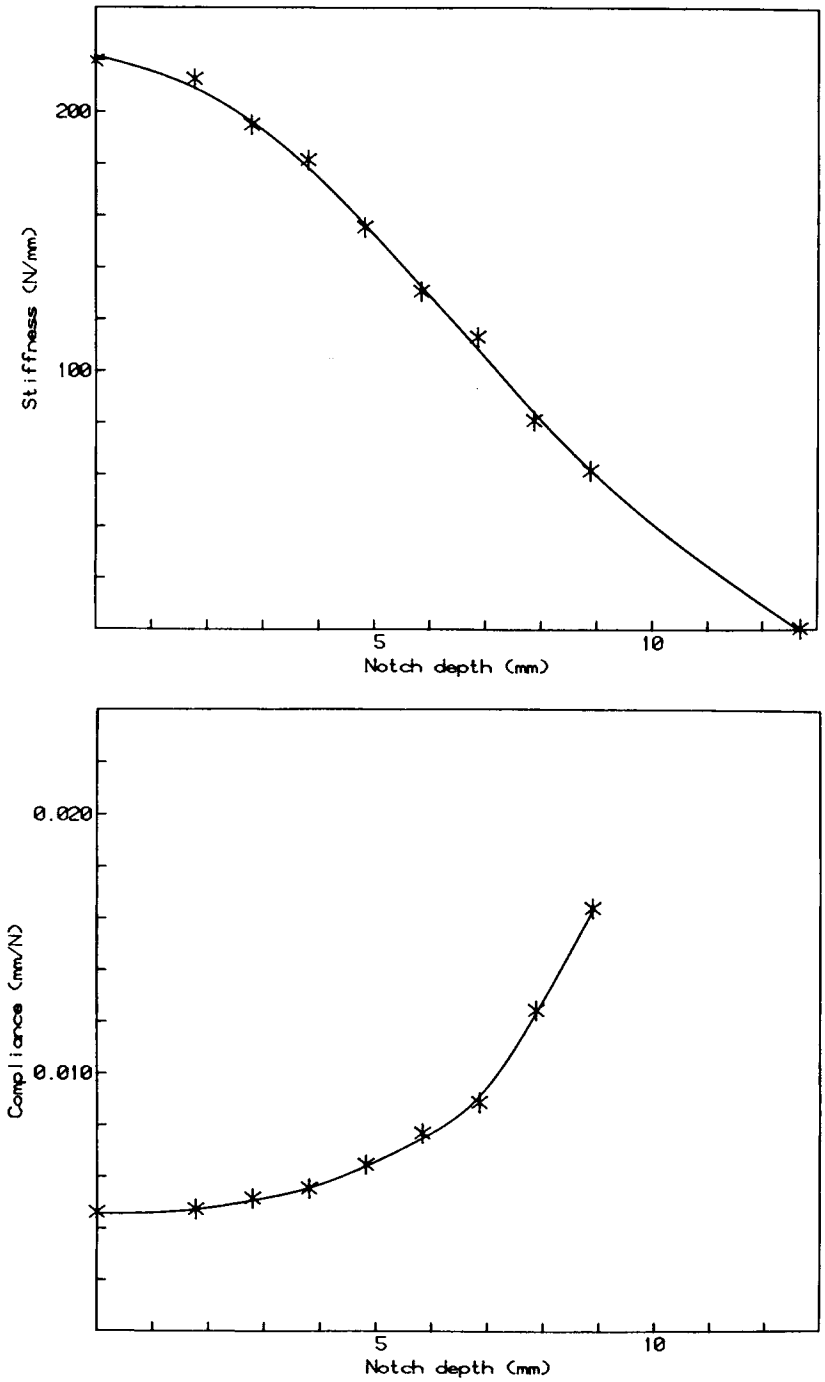

Fig. 5(a). Slope data from Figure 3 expressed as stiffness (dP/dv) as a function of notch depth. (b). Slope data from Figure 3 expressed as compliance (dv/dP) as a function of notch depth.

conclude that v_c is asymptotic as the notch depth approaches the specimen width with a nonzero asymptote.

The slopes of the corrected P–v curves of Figure 3 represent the stiffness γ of each of the specimens tested. The inverse-slope will therefore represent the compliance C of the specimens. Both the stiffness γ and the compliance C are plotted as a function of the notch depth a in Figures 5(a) and 5(b), respectively. Again, smooth curves using natural splines are drawn on both the plots. Figure 5(a) shows an inflection point at notch depth of 6.35 mm (specimen half-width) where the curvature changes sign from negative to positive. This is a manifestation of unstable/stable crack propagation and correlates well with the observed change in the stability of crack growth.

DISCUSSION

As mentioned earlier, the goal of this work is to compare the constancy of the critical values of the parameters σ_{max}, K, G, and J for a range of notch depths. To make such a comparison, we need operational definitions of each of these parameters so that we can compute their numerical values at the onset of crack growth in each specimen. We have used the following definitions based on the fundamental concepts involved in developing these parameters.[33,34]

Using linear elastic fracture mechanics, the J-integral is evaluated from the following expression:

$$J_I = -(1/2t)v^2(d\gamma/da)$$

Since the compliance of the testing apparatus is negligible compared to the compliance of the specimen, v in this experiment is identified with the load point displacement. As v approaches the displacement $v_c(a)$ at which crack growth initiates, J_I approaches the critical value J_{Ic}.

Similarly, the energy release rate G_I, is evaluated from the following expression:

$$G_I = (1/2t)P^2(dC/da)$$

and, as P approaches the critical value $P_c(a)$, G_I should approach the critical value G_{Ic}. We expect J_{Ic} and G_{Ic} to be numerically equal. They are identical for ideal linear elastic solids. In the equations above, $d\gamma/da$ and dC/da were found from the fitted curves of γ vs. a [Fig. 5(a)] and C vs. a [Fig. 5(b)], respectively.

The stress-intensity factor K_I is evaluated from the following expression:

$$K_I = \sigma_n(\pi a)^{0.5} f(a/w)$$

where

$$\sigma_n = 3Ps/tw^2$$

and $f(a/w)$ is a geometric factor computed employing numerical techniques.[35]

The stress at the notch tip, σ_{loc}, is calculated from the following expression:

$$\sigma_{loc} = \alpha_{k'}\sigma_{nom}$$

where

$$\sigma_{\text{nom}} = 3Ps/t(w-a)^2$$

and as P approaches the critical value $P_c(a)$, σ_{loc} approaches the critical value σ_c. The stress concentration factor $\alpha_{k'}$, as defined by Neuber, is computed from α_{fk} for shallow notches and from α_{tk} for deep notches with the following expression:

$$\alpha_{k'} = \frac{(\alpha_{fk}-1)(\alpha_{tk}-1)}{\left[(\alpha_{fk}-1)^2+(\alpha_{tk}-1)^2\right]^{0.5}} + 1$$

where α_{fk} and α_{tk} are given by

$$\alpha_{fk} = 1 + 2(t/\rho)^{0.5} \qquad \text{for } a \ll w$$

$$\alpha_{tk} = \frac{2(b/\rho+1) - \alpha_1(b/\rho+1)^{0.5}}{4\alpha_2(b/\rho+1) - 3\alpha_1} \qquad \text{for } (w-a) \ll w$$

where

$$\alpha_1 = \frac{2(b/\rho+1)(b/\rho)^{0.5}}{(b/\rho+1)\tan^{-1}(b/\rho)^{0.5} + (b/\rho)^{0.5}}$$

$$\alpha_2 = \frac{4(b/\rho)^{0.5}}{3\left[(b/\rho+1)\tan^{-1}(b/\rho)^{0.5} + (b/\rho)^{0.5}\right]}$$

In all the above expressions, t (= 6.35 mm) is the thickness, w (= 12.7 mm) is the width of the specimen, a is the notch depth, $b = w - a$ is the remaining ligament width, and ρ (= 0.25 mm) is the notch tip radius.

In each case, there may be restrictions on sample size, notch geometry, etc. in testing metallic materials. To make our comparison, we have relaxed these restrictions. This should not lead to any difficulties, however, given the strongly brittle characteristics of the styrene material.

The critical values of the above parameters, J_{Ic}, G_{Ic}, K_{Ic}, and σ_c, were calculated for each notch depth. The mean critical value and the standard deviation were also calculated for each of these parameters. In order to study the constancy of these parameters, the ratio of critical value to its mean value is plotted against the notch depth in Figure 6.

From Figure 6, it is evident that σ_c is most constant for the range of notch depths studied. That is, it is the best predictor of the onset of crack propagation over a range of notch depths. Further, J_{Ic} and G_{Ic} are not only unequal but also show a large scatter. If we were forced to rank these parameters as material properties in their ability to predict fracture initiation, then, based on our experimental results, σ_c would rank as the best criterion, with K_{Ic} being a close second, followed by J_{Ic} and G_{Ic}.

The J-integral approach, however, is useful in predicting the fracture mode during crack propagation. The neutral mechanical stability of a propagating

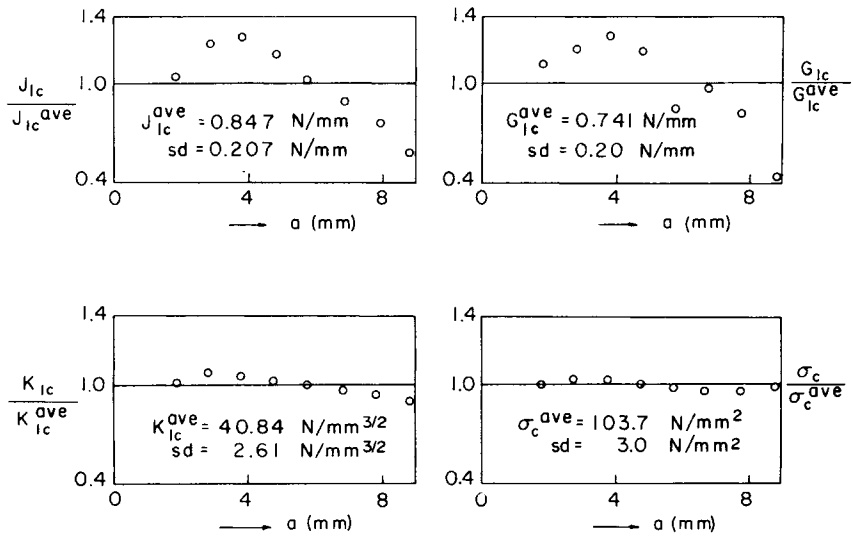

Fig. 6. Comparison of parameters at the onset of fracture as a function of notch depth. Solid lines represent the mean values. Note that all plots have been normalized by the corresponding mean values.

crack under constant displacement testing conditions has been studied by Burns.[36] It is suggested that crack propagation behavior changes when

$$(\partial J_I/\partial a)_{v=\text{const}} = 0 = (\partial^2\gamma/\partial a^2)$$

In other words, when curvature of γ vs. a curve [Fig. 5(a)] changes sign. This occurs at $a = 6.35$ mm, and was experimentally observed. For notch depths greater than 6.35 mm, the crack propagated a small distance before it was arrested due to the resulting load drop. A load increase was required to propagate it further.

SUMMARY AND CONCLUSION

The four-point bend test performed on notched polystyrene specimens gives consistent results for both the stress–strain behavior and the fracture initiation mechanisms operative in the material. The material, Styron 678U, was found to be linear elastic and brittle. If we were to index the various parameters to predict fracture initiation in Styron 678U based on the constancy of critical values over a range of notch depths, the stress concentration at the notch tip appears to be the best criterion, with the stress-intensity factor K_{Ic} being a close second. There is a clear onset of instability in crack propagation for notch depths smaller then 6.35 mm (half-width of specimens). This correlates extremely well with the curvature of stiffness vs. notch depth curve changing sign at $a/w = 0.5$.

We wish to acknowledge the support of the Mechanical Engineering Departments of the Rochester Institute of Technology and the University of Rochester for allowing us to use their facilities for specimen preparation and testing. We also wish to thank the reviewer for his comments and criticism.

References

1. W. F. Brown, Jr., *ASTM STP*, **463** (1970)
2. P. C. Paris, H. Ernst, and C. E. Turner, *ASTM STP*, **700**, 338 (1980).
3. M. G. Vassilaros, J. A. Joyce, and J. P. Gudas, *ASTM STP*, **700**, 251 (1980).
4. A. N. Gent, *J. Mater. Sci.*, **5**, 925 (1970).
5. A. S. Argon and J. G. Hanoosh, *Phil. Mag.*, **36**(5), 1195 (1977).
6. A. S. Argon and J. G. Hanoosh, *Phil. Mag.*, **36**(5), 1217 (1977).
7. B. D. Lauterwasser and E. J. Kramer, *Phil. Mag.*, **A39**(4), 469 (1979).
8. J. G. Williams, *Adv. Polym. Sci.*, **27**, 69 (1978).
9. E. H. Andrews and P. E. Reed, *Adv. Polym. Sci.*, **27**, 1 (1978).
10. H. R. Brown, *J. Mater. Sci.*, **17**, 469 (1982).
11. J. G. Williams, *Fracture Mechanics of Polymers*, Ellis Harwood, London, 1984.
12. A. J. Kinloch and R. J. Young, *Fracture Behavior of Polymers*, Applied Science, London, 1983.
13. J. R. Rice, in *Fracture: An Advanced Treatise*, H. Liebowitz, Ed., Academic, New York, 1970, p. 191.
14. J. F. Knott, *Fundamentals of Fracture Mechanics*, Butterworths, London, 1973.
15. B. R. Lawn and T. R. Wilshaw, *Fracture of Brittle Solids*, Cambridge University Press, Cambridge, 1975.
16. ASTM Standard E813-81, Standard test for J_{Ic}, a measure of fracture toughness, 1981.
17. ASTM Standard E399-81, Standard test methods for plane strain fracture toughness of metallic materials, 1981.
18. H. Neuber, *Theory of Notch Stresses: Principles for Exact Stress Calculation*, translated by F. A. Raven, Translation 74, US Navy, Washington, DC, 1945.
19. G. R. Irwin, in *Encyclopedia of Physics*, S. Flügge, Ed., Springer-Verlag, Berlin, 1958, Vol. 6, p. 551.
20. G. R. Irwin, *J. Appl, Mech.*, **24**, 361 (1957).
21. J. A. Begley and J. D. Landes, *ASTM STP*, **514**, 1 (1972).
22. R. J. Bucci, P. C. Paris, J. D. Landes, and J. R. Rice, *ASTM STP*, **514**, 40 (1972).
23. R. P. Kambour, *J. Polym. Sci., Macromol. Rev.*, **7**, 1 (1973).
24. R. P. Kambour, *J. Polym. Sci., A-2*, **4**, 17 (1966).
25. R. P. Kambour, *J. Polym. Sci., A-2*, **4**, 349 (1966).
26. J. Murray and D. Hull, *J. Polym. Sci., A-2*, **8**, 583 (1970).
27. A. N. Gent, *J. Macromol. Sci. Phys.*, **B8**(3–4), 597 (1973).
28. A. M. Donald and E. J. Kramer, *Phil. Mag. A*, **43**(4), 857 (1981).
29. Dow Chemicals, "STYRON 678U—polystyrene resins," Form 301-388-77, Midland, MI.
30. R. M. Kucejko, M.S. thesis, University of Rochester, 1981.
31. J. K. Wittmershaus, M.S. thesis, University of Rochester, 1985.
32. *IMSL User's Manual, Cubic Spline Data Smoother (Easy to Use Version)*, edition 9.2, IMSL Inc., Houston, ICSSCV-1, 1984, Vol. 2.
33. J. W. Hutchinson, in *Nonlinear Fracture Mechanics*, Department of Solid Mechanics, Technical University of Denmark, 1979.
34. K. Hellan, in *Introduction to Fracture Mechanics*, McGraw-Hill, New York, 1984.
35. H. Tada, P. C. Paris, and G. R. Irwin, in *The Stress Analysis of Cracks Handbook*, Del Research Corp. 1973.
36. S. J. Burns, in *Environmental Degradation of Engineering Materials in Aggressive Environments*, M. R. Louthan, Jr., et al., Eds., Virginia Polytechnic Institute, Blacksburg, VA, 1981, p. 543.

Received August 12, 1985
Accepted February 14, 1986